

Magnetomechanical Torques in Small Magnetic Cantilevers

Alexey A. Kovalev,¹ Gerrit E. W. Bauer,¹ and Arne Brataas²

¹*Kavli Institute of NanoScience, Delft University
of Technology, 2628 CJ Delft, The Netherlands*

²*Department of Physics, Norwegian University of
Science and Technology, N-7491 Trondheim, Norway*

(Dated: 1st July 2021)

Abstract

We study the dynamics of small magnetic cantilevers, either made from Si covered by a magnetic film or entirely ferromagnetic ones. The magnetomechanical torques are found to cause line splittings in ferromagnetic resonance spectra and magnetization reversal facilitated by mechanical degrees of freedom. We show that the magnetomechanical torques can extend the limits of detecting and exciting motion at the nanoscale. A "nanomotor" described here effectively transforms rf magnetic fields into mechanical oscillations. We furthermore propose to integrate mechanical oscillators into magnetoelectronic devices that make use of current-induced spin-transfer torques. This opens new possibilities for electric transducers of nanomechanical motion.

PACS numbers:

I. INTRODUCTION

Micro- and nanoelectromechanical systems (NEMS)^{1,2} allow nanoscale control over as small sensors with spatial resolution on an atomic scale³ operating at frequencies in the GHz range.⁴ NEMS detection of extremely small forces corresponding to biomolecular interactions⁵ and mass changes corresponding to single molecules⁶ have been reported. Efforts have been made to merge the field of nanomechanics with that of nanoscale magnetism. The success in the detection of a single electron spin by magnetic resonance is a good example.⁷ A nuclear spin sensor that is based on imposing a coherent motion on nuclear spins has been proposed.⁸ Here we focus on the possibilities provided by the coupled motion of the strain field of a cantilever and the magnetization of a ferromagnet.^{9,10} Magnetization reversal in small magnetic clusters¹¹ is usually realized by external magnetic fields^{12,13,14,15} or polarized spin currents employing spin-transfer torques.^{16,17,18,19,20,21,22,23} Along alternative mechanisms to switch the magnetization such as employing antiferromagnets²⁴ and time-dependent magnetic fields²⁵, we suggest the effect of mechanically assisted magnetization reversal.¹⁰ The fastest mechanical device reported in the literature is operated with the help of magnetomotive forces at GHz frequencies.⁴ We propose to actuate such systems by demagnetizing currents that provide coupling between the mechanical and the magnetization motion most efficiently in the GHz range. Coupling of the magnetization motion to an electric circuit via spin-transfer torques and magnetoresistance then opens the possibility of high frequency transducers of nanomechanical motion. In this paper, we report consequences for the magnetovibrational coupling such as splitting of the ferromagnetic resonance (FMR) spectrum and magnetization reversal facilitated by the mechanical degrees of freedom. We argue that a predominantly ferromagnetic cantilever provides stronger coupling and, when integrated into a magnetoelectronic circuit, offers new functionalities for both mechanical and magnetic devices. Some preliminary results have been reported already.^{9,10}

The paper is organized as follows. In Sec. II, we describe our system, the magnetic cantilever, and derive a set of equations describing magnetomechanical motion. In Sec. III, we solve these equations in the limit of small magnetization oscillations, finding a splitting of FMR spectra for the resonantly coupled mode. In Sec. IV, we propose a current-induced magnetic resonance technique in spin valves and demonstrate that magnetovibrational modes can be detected by this method. Finally, in Sec. V, we analyze large magnetization os-

cillations in the presence of magnetovibrational couplings and demonstrate magnetization reversal assisted by the mechanical degrees of freedom.

II. SYSTEM

We consider first a small dielectric cantilever with a single-domain ferromagnetic layer deposited on its far end (see Fig. 1). A constant external field \mathbf{H}_0 is applied along the z axis. In section 3, we also include an oscillating field H_y along the y axis to pump and probe the system. The effective field \mathbf{H}_{eff} felt by the magnetization consists of \mathbf{H}_0 as well as the crystal anisotropy and the demagnetizing fields. The strains are localized in the mechanical link of the cantilever between the ferromagnetic film at one end and the other end that is fixed. The lattice of the ferromagnet then oscillates without internal mechanical strains, but crystalline and form anisotropies couple the magnetic order parameter to the torsional mode of the cantilever.

Our setup consists of two weakly interacting subsystems - the magnetic and the mechanical. It is then useful to first study the two subsystems separately.

A. Magnetization motion in a single-domain ferromagnet

The magnetization \mathbf{M} of the ferromagnet precesses around an effective magnetic field \mathbf{H}_{eff} according to the Landau-Lifshitz-Gilbert equation:²⁶

$$\frac{d\mathbf{M}}{dt} = -\gamma\mathbf{M} \times \mathbf{H}_{\text{eff}} + \frac{\alpha}{M_s}\mathbf{M} \times \frac{d\mathbf{M}}{dt}, \quad (1)$$

where γ denotes the gyromagnetic ratio. The phenomenological Gilbert constant is typically $\alpha \lesssim 0.01$ for metallic and $\alpha \lesssim 0.00001$ for insulating ferromagnets. The effective field is given by the functional derivative of the free energy of the system, that is of the form (in the lowest order in magnetizations in some specially chosen reference frame)

$$E_{mg} = \frac{1}{2}D_x M_x^2 + \frac{1}{2}D_y M_y^2 + \frac{1}{2}D_z M_z^2 - \mathbf{M}\mathbf{H}_0, \quad (2)$$

where D_x , D_y and D_z describe the anisotropy of the magnetization along the Cartesian axes x , y and z , including demagnetizing effects and crystalline anisotropy. The associated effective field is given by $\mathbf{H}_{\text{eff}} = \mathbf{H}_0 - D_x M_x \mathbf{x} - D_y M_y \mathbf{y} - D_z M_z \mathbf{z}$.

B. Small magnetization oscillations and dependence of FMR broadening on shape and crystal anisotropies

To first order, the deviations from the equilibrium magnetization in the z -direction lie in the $x-y$ plane: $\mathbf{M} = m_x \mathbf{x} + m_y \mathbf{y} + M_s \mathbf{z}$, where M_s is the saturation magnetic moment. The magnetic susceptibilities $\chi_{yy}(\omega) = (m_y/H_y)_\omega$ and $\chi_{yx}(\omega) = (m_x/H_x)_\omega$ describe the linear response of the magnetization m_y to a (weak) rf magnetic field H_y (H_x) at frequency ω and can be found after linearizing the LLG equation in frequency space:

$$\chi_{yy}(\omega) = \frac{\gamma^2 M_s (H_0 + (D_x - D_z) M_s)}{\omega^2 - (1 + \alpha^2) \omega_m^2 + i \alpha \omega (2H_0 + (D_x + D_y - 2D_z) M_s)}, \quad (3)$$

$$\chi_{yx}(\omega) = \frac{i \omega \gamma M_s}{\omega^2 - (1 + \alpha^2) \omega_m^2 + i \alpha \omega (2H_0 + (D_x + D_y - 2D_z) M_s)}, \quad (4)$$

where $\omega_m^2 = (H_0 + (D_x - D_z) M_s)(H_0 + (D_y - D_z) M_s)$ is the FMR resonant frequency. Note that the FMR damping has to be renormalized in the presence of anisotropies. The broadening of the FMR lineshape is

$$\alpha' = \alpha \frac{(H_0/M_s + (D_x + D_y)/2 - D_z)}{\sqrt{(H_0/M_s + D_x - D_z)(H_0/M_s + D_y - D_z)}}$$

Let us consider an ellipsoid with the semi-axes a and $b = c$. For small crystalline anisotropies the anisotropy factors are defined by shape anisotropies

$$\begin{aligned} D_x &= \frac{4\pi}{m^2-1} \left[\frac{m}{2\sqrt{m^2-1}} \ln\left(\frac{m+\sqrt{m^2-1}}{m-\sqrt{m^2-1}}\right) - 1 \right] \stackrel{m \ll 1}{\approx} 4\pi - 2\pi m, \\ D_y = D_z &= \frac{2\pi m}{m^2-1} \left[m - \frac{1}{2\sqrt{m^2-1}} \ln\left(\frac{m+\sqrt{m^2-1}}{m-\sqrt{m^2-1}}\right) \right] \stackrel{m \ll 1}{\approx} \pi m, \end{aligned} \quad (5)$$

where $m = a/c$. The dependence of FMR broadening on the aspect ratio m is plotted in Fig. 2.

C. Nonlinear magnetization oscillations

Without Gilbert damping the dynamics of the magnetization can be analyzed analytically for different magnetic anisotropies²⁷. We present here solutions for the ‘‘easy plane’’ anisotropy when $D_y = D_z = 0$ and $\mathbf{H}_0 = H_0 \mathbf{z}$ which is relevant for Section 4. Without the

Gilbert damping but including the anisotropy factor D_x the LLG equations read

$$\begin{cases} \frac{dM_x}{dt} = -\gamma M_y H_0 \\ \frac{dM_y}{dt} = \gamma M_x H_0 + \gamma D_x M_z M_x \\ \frac{dM_z}{dt} = \gamma D_x M_y M_x \end{cases} \quad (6)$$

The x -component of the magnetization then obeys

$$\ddot{M}_x = -(H_0^2 - D_x E_{mg})\gamma^2 M_x - \frac{\gamma^2}{2} D_x^2 M_x^3 \quad (7)$$

where the energy $E_{mg} = -H_0 M_z + D_x M_x^2/2$ is constant when there is no Gilbert damping.

This equation describes a so-called ‘‘Duffing oscillator’’, one of the rare examples of a non-linear dynamic systems that can be solved analytically. The potential energy of the oscillator has two minima. As a result, one can observe effects like periodic motion centered at one of those minima that with increasing energy suddenly doubles its period. When a periodic external force is applied to such an oscillator, the system may carry out jumps between minima leading to stochastic motion in time. Duffing’s equation

$$\ddot{x} - kx + 2\lambda x^3 = 0 \quad (8)$$

can be integrated at once to give the first integral:

$$\dot{x}^2 - kx^2 + \lambda x^4 = Z, \quad (9)$$

where Z is the energy of the Duffing oscillator. By comparing Eqs. (6,7) to Eqs. (8,9) we obtain that $Z = \gamma^2(M^2 H_0^2 - E_{mg}^2)$, $k = \gamma^2(D_x E_{mg} - H_0^2)$ and $\lambda = \gamma^2 D_x^2/4$. The energy minima of the Duffing oscillator therefore correspond to the energy maxima in our system. One can distinguish three different types of solutions.

1. $Z < 0$. ‘‘Small amplitude’’ solutions when motion is at energies close to an energy minimum (in Fig. 3 it corresponds to two small circles and $E_{mg} > 1$, the magnetization oscillates close to the perpendicular to the film direction). We express the solutions in terms of Jacobi elliptic functions dn:

$$x = \sqrt{\frac{k}{\lambda(2-v^2)}} \operatorname{dn} \left(\sqrt{\frac{k}{\lambda(2-v^2)}} t, v \right) \quad (10)$$

where v can be found from $Z = -\frac{k^2(1-v^2)}{4\lambda(1-v^2/2)^2}$.

2. $Z = 0$ corresponds to the separatrix (in Fig. 3 it is the longest possible trajectory in a shape of a bent "8"). Here the Jacobi functions degenerate to hyperbolic function ch:

$$x = \pm \sqrt{\frac{k}{\lambda}} \frac{1}{\text{ch}(kt)} \quad (11)$$

3. $Z > 0$ (in Fig. 3 it corresponds to bent elliptical trajectories and $E_{mg} < 1$, the magnetization trajectories are squeezed in the perpendicular to the film direction). "Large amplitude" solutions via the Jacobi functions cn:

$$x = \sqrt{\frac{k}{\lambda(2v^2 - 1)}} v \text{cn} \left(\sqrt{\frac{k}{\lambda(2v^2 - 1)}} t, v \right) \quad (12)$$

where $Z = -\frac{k^2 v^2 (1-v^2)}{\lambda(2v^2-1)^2}$.

The analytical solution in our case can be written for the entire parameter space with the exception of the separatrix by a single formula as follows:

$$M_x = \sqrt{-2p_-} \text{dn} \left(t\gamma\sqrt{-p_-/2}, 1 - p_+/p_- \right)^{p_- \ll p_+} \approx \sqrt{-2p_-} \cos(t\sqrt{p_+/2}) \quad (13)$$

$$M_y = -\frac{\dot{M}_x}{\gamma H_0}, \quad M_z = \frac{D_x M_x^2 - 2E_{mg}}{2H_0}, \quad (14)$$

where $p_{\pm} = H_0^2 - D_x E_{mg} \pm H_0 \sqrt{H_0^2 - 2D_x E_{mg} + D_x^2 M_s^2}$. When $D_x > 0$ this leads to the trajectories and oscillation periods depicted in Fig. 3. The motion is periodic with time periods that can be expressed by elliptic integrals K as

$$\begin{aligned} T_1 &= 4\sqrt{2}K(p_-/p_+) / (\gamma\sqrt{p_+})^{p_- \ll p_+} \approx 2\pi\sqrt{2/p_+}; & E_{mg} < MH_0 \\ T_2 &= 2\sqrt{2}K(1 - p_+/p_-) / (\gamma\sqrt{-p_-})^{|p_- - p_+| \ll |p_-|} \approx \pi\sqrt{-2/p_-}. & E_{mg} > MH_0 \end{aligned} \quad (15)$$

The variation of the periodicity has important consequence for the coupling to the lattice in the regime of large magnetization oscillations as explained below.

D. Cantilever oscillations and coupled magneto-mechanical equations

Throughout this paper, we assume that the torsional oscillations of the cantilever are small. The torsional motion of the part of the cantilever that is not covered by the ferromagnet can be found by applying the variational principle to the total elastic energy:²⁸

$$E_{el} = \frac{1}{2} \int_0^L C \tau^2 dy, \quad (16)$$

where $\tau = \partial\varphi/dy$ and C is an elastic constant defined by the shape and material of the cantilever ($C = \frac{1}{3}\mu da^3$ for a plate with thickness a much smaller than width d , $a \ll d$, μ is the Lamé constant). $T = C\tau(y)$ is the torque flowing through the cantilever at point y . The integration is taken from the clamping point $y = 0$ until the cantilever endpoint $y = L$. The equation of motion reads

$$C \frac{\partial^2 \varphi}{\partial y^2} = \rho I \frac{\partial^2 \varphi}{\partial t^2} + 2\beta \rho I \frac{\partial \varphi}{\partial t}, \quad (17)$$

where $I = \int (z^2 + x^2) dz dx \simeq ad^3/12$ is the moment of inertia of the cross-section about its center of mass, ρ the mass density, and β is a phenomenological damping constant related to the quality factor Q at the resonance frequency ω_e as $Q = \omega_e/(2\beta)$ (at 1 GHz $Q \sim 500$).⁴ Note that ω_e can be also a higher harmonic resonance frequency in what follows. The oscillating solution has the form $\varphi = \sin(ky)(A_1 \sin(\omega t) + A_2 \cos(\omega t))$, where $k = (\omega + i\beta)/c$ is the wave number, $c = c_t 2h/d = \sqrt{C/(\rho I)}$ and $c_t = \sqrt{\mu/\rho}$ is the transverse velocity of sound. The free constants A_1 and A_2 depend on the initial conditions. The boundary condition $\varphi|_{y=0} = 0$ at the clamping point is already fulfilled, and the boundary condition at the end $y = L$ is discussed in the following.

Combining Eqs. (2,16) and taking into account the smallness of the magnet $\Delta L \ll L$ we can write the free energy of the cantilever coupled to the magnetization:

$$F = V(-\mathbf{M}\mathbf{H}_0 + \frac{D_x}{2} [M_x + M_z\varphi(L)]^2 + \frac{D_z}{2} [M_z - M_x\varphi(L)]^2 + \frac{D_y M_y^2}{2}) + \frac{C}{2} \int_0^L \tau^2 dy. \quad (18)$$

Eq. (18) demonstrates that magneto-mechanical coupling is only possible when the factors D_x or D_z are non-zero (the anisotropy factor D_y does not contribute to the coupling since our mechanical motion is rotationally invariant with respect to the axis y and one needs anisotropies D_x and D_z to break the invariance). For small $\varphi = \varphi(L)$, where $\varphi(y)$ is the torsion angle at position y of the cantilever, the effective field $\mathbf{H}_{\text{eff}} = -\frac{\partial F}{\partial \mathbf{M}}$ is

$$\mathbf{H}_{\text{eff}} = (D_x M_z \varphi - D_x M_x) \mathbf{x} + D_x M_x \varphi \mathbf{z} - (D_z M_x \varphi + D_z M_z) \mathbf{z} - D_z M_z \varphi \mathbf{x} - D_y M_y + \mathbf{H}_0$$

where D_x , D_y and D_z describe the anisotropies ($D_x \simeq 4\pi$ for a thin film without crystal anisotropies). The equation of motion of the magnetization \mathbf{M} in the presence of the mechanical degree of freedom then reads

$$\frac{d\mathbf{M}}{dt} = -\gamma \mathbf{M} \times \mathbf{H}_{\text{eff}} + \frac{\alpha}{M_s} \mathbf{M} \times \left(\frac{d\mathbf{M}}{dt} \right)_{\text{cant}}, \quad (19)$$

where the derivative $(\frac{d\mathbf{M}}{dt})_{\text{cant}} = \frac{d\mathbf{M}}{dt} + \frac{d\varphi}{dt}(-M_z\mathbf{x} + M_x\mathbf{z})$ is taken in the reference system of the cantilever since the magnetization damping is caused by interactions of the magnetization with the bulk of the cantilever.

By applying the variational principle to Eq. (18) we obtain Eq. (17) and the second boundary condition for its solutions. The magnetovibrational coupling can then be treated as a boundary condition to the mechanical problem, which is expressed as the torque $C\tau|_{y=L}$ exerted by the magnetization on the edge of the cantilever:

$$C\tau|_{y=L} = \frac{1}{\gamma} \left(\frac{d\mathbf{M}}{dt} + \gamma\mathbf{M} \times \mathbf{H}_0 \right) |_{y=L}, \quad (20)$$

This boundary condition is equivalent to the conservation law of the mechanical angular momentum written for the tip of the cantilever. Let us introduce an angular momentum $\mathbf{V}^{\text{el}}(y)$ for a thin slice at point $y \in \{0, L\}$ (without magnetic overlayer), then the conservation law is $d\mathbf{V}^{\text{el}}(y)/dt = \mathbf{T}(y)$, where $\mathbf{T}(y)$ is the torque flowing into the slice. This equation is modified by the coupling to the magnet in a region $y \in \{L, L + \Delta L\}$ (ΔL is the length of the cantilever covered by the magnetic layer) as:

$$\frac{d}{dt} \left(\mathbf{V}^{\text{el}}(L) + \left(-\frac{1}{\gamma}\right)\mathbf{M}(L)V \right) = \mathbf{T}(L) + \mathbf{T}_{\text{field}}. \quad (21)$$

where $\mathbf{T}_{\text{field}} = V\mathbf{M} \times \mathbf{H}_0$, V is the volume of the magnet and $\mathbf{T}(y)|_y = -C\tau(y)$. When $\Delta L \ll L$, internal strains in the magnetic section may be disregarded and the magnetization torque can be treated as a boundary condition Eq. (20).

The coupling of Eqs. (1) and (17) can be made explicit:

$$\begin{aligned} \partial\varphi/dy|_{y=L} &= \frac{1}{C\gamma} \left(\frac{dM_y}{dt} + \gamma\mathbf{M} \times \mathbf{H}_0 \right) \\ \mathbf{H}_{\text{eff}} &= (D_x M_z \varphi - D_x M_x) \mathbf{x} + D_x M_x \varphi \mathbf{z} - (D_z M_x \varphi + D_z M_z) \mathbf{z} - D_z M_z \varphi \mathbf{x} - D_y M_y + \mathbf{H}_0 \end{aligned} \quad (22)$$

E. Entirely ferromagnetic cantilever

It is straightforward to generalize the free energy Eq. (18) to the case when the whole cantilever is covered by a ferromagnetic film or when the whole cantilever is ferromagnetic. The free energy then has the form:

$$F = V(-\mathbf{M}\mathbf{H}_0 + \frac{D_x}{2} [M_x + M_z\bar{\varphi}]^2 + \frac{D_z}{2} [M_z - M_x\bar{\varphi}]^2 + \frac{D_y M_y^2}{2}) + \frac{C}{2} \int_0^L \tau^2 dy \quad (23)$$

where $\bar{\varphi} = \frac{1}{L} \int_0^L \varphi(y) dy$ is the average angle of torsion. In this case the system of the magnetomechanical equations becomes:

$$\begin{aligned} \frac{d\mathbf{M}}{dt} &= -\gamma \mathbf{M} \times \mathbf{H}_{\text{eff}} + \frac{\alpha}{M_s} \mathbf{M} \times \left(\frac{d\mathbf{M}}{dt} \right)_{\text{cant}} \\ C \frac{\partial^2 \varphi}{\partial y^2} &= \rho I \frac{\partial^2 \varphi}{\partial t^2} + \frac{S}{\gamma} \left(\frac{dM_y}{dt} + \gamma \mathbf{M} \times \mathbf{H}_0 \right) + 2\beta \rho I \frac{\partial \varphi}{\partial t} \\ C \partial \varphi / dx|_{x=L} &= 0 \end{aligned}$$

$$\mathbf{H}_{\text{eff}} = (D_x M_z \bar{\varphi} - D_x M_x) \mathbf{x} + D_x M_x \bar{\varphi} \mathbf{z} - (D_z M_x \bar{\varphi} + D_z M_z) \mathbf{z} - D_z M_z \bar{\varphi} \mathbf{x} - D_y M_y + \mathbf{H}_0 \quad (24)$$

The coupling can be much more efficient in the latter as compared to the former system since the volume of the magnet is larger. The disadvantage is that the form anisotropy wants to align the magnetization along the cantilever making the subsystems uncoupled. Another disadvantage, the possibility of spin wave excitations, is discussed in the next section.

III. SMALL MAGNETIZATION OSCILLATIONS

A. Magnet at the tip of cantilever

To first order, the deviations from the equilibrium magnetization in the z -direction lie in the $x - y$ plane: $\mathbf{M} = m_x \mathbf{x} + m_y \mathbf{y} + M_s \mathbf{z}$, where M_s is the saturation magnetic moment (see Fig. 1). For small φ , the effective field oscillates in the $x - y$ plane: $\mathbf{H}_{\text{eff}} = (D_x M_s \varphi - D_x M_x) \mathbf{x} + D_x M_x \varphi \mathbf{z} - (D_z M_x \varphi + D_z M_s) \mathbf{z} - D_z M_s \varphi \mathbf{x} - D_y M_y + \mathbf{H}_0$, ($D_x \simeq 4\pi$ for a thin film without crystal anisotropy). Note that the coupling does not rely on a strong magnetocrystalline field, since the surface forces of demagnetizing currents also provide a restoring torque. For a thin ferromagnetic layer the latter dominates and the magnetization does not precess, but oscillates like a pendulum in the $y - z$ plane due to the oscillating field in the x -direction $\mathbf{H}_{\text{eff}} = D_x M_s \varphi \mathbf{x}$.

By using Eq. (20) with the substitution of φ in τ , $C\tau|_{y=L} = Ck \cos(kL)(A_1 \sin(\omega t) + A_2 \cos(\omega t)) = Ck\varphi \cot(kL)$, we obtain in frequency space and to first order in the magnetization oscillations:

$$Ck\varphi \cot(kL) = \frac{V}{\gamma} (-i\omega m_y - \gamma H_0 m_x) \quad (25)$$

$$\approx -C\varphi \frac{L}{2c^2} (\omega^2 + 2i\beta\omega - \omega_e^2), \quad (26)$$

where in the second line the cot has been expanded close to the resonance frequency $\omega_e =$

$c\pi(1/2 + s)/L$ (s is integer, here we concentrate mainly on coupling to the first harmonic and $s = 0$).

The magnetic susceptibilities $\chi_{yy}(\omega) = (m_y/H_y)_\omega$ and $\chi_{yx}(\omega) = (m_y/H_x)_\omega$ describe the linear response of the magnetization m_y to a (weak) rf magnetic field $H_y(H_x)$ at frequency ω . Generalization of Eqs (3,4) in the presence of magneto-vibrational coupling can be found after writing LLG equation in frequency space with use of Eq. (25), and taking into account smallness of the Gilbert damping α :

$$\chi_{yy}(\omega) = \frac{\gamma^2 M_s^2 (D_x - D_z + H_0(1 - g \tan(kL)))/M_s}{\omega^2 - \omega_m^2 + 2i\alpha'\omega\omega_m + [\omega^2 - H_0(H_0 + (D_y - D_z)M_s)] g \tan(kL)} \quad (27)$$

$$\chi_{yx}(\omega) = \frac{i\omega\gamma M_s}{\omega^2 - \omega_m^2 + 2i\alpha'\omega\omega_m + [\omega^2 - H_0(H_0 + (D_y - D_z)M_s)] g \tan(kL)} \quad (28)$$

where $g = M_s^2 V (D_x - D_z) c^2 / (CL\omega_e^2) = (2/\pi)^2 (D_x - D_z) (L/a)^2 (V/V_c) (M_s^2/\mu)$ is the magneto-vibrational coupling constant (V and V_c are the volumes of the magnet and the cantilever respectively) and the unperturbed resonance frequency $\omega_m^2 = (H_0 + (D_x - D_z)M_s)(H_0 + (D_y - D_z)M_s)$. Note that the coupling constant is defined by the material parameters in the term M_s^2/μ , by the geometry in the term $(L/a)^2 (V/V_c)$ and by both the geometry and the material parameters in the term $(D_x - D_z)$. The imaginary part of $\chi_{yy}(\omega)$ is proportional to the FMR absorption signal.

When the cantilever with the magnet is subjected to the rf magnetic field, the magnetomechanical torques induce a mechanical motion. In effect we have then constructed a nano-scale motor that transforms the magnetic field oscillations into mechanical motion with amplitudes that are given by the susceptibility $\chi_{\varphi y}(\omega) = (\varphi/H_y)_\omega$. The latter follows from the LLG equation in frequency space using Eq. (25), and taking into account the smallness of the Gilbert damping α :

$$\chi_{\varphi y}(\omega) = \frac{i\omega g \tan(kL)}{\omega^2 - \omega_m^2 + 2i\alpha'\omega\omega_m + [\omega^2 - H_0(H_0 + (D_y - D_z)M_s)] g \tan(kL)} \quad (29)$$

In the absence of the external field H_0 the resonance frequencies in the vicinity of the resonance frequency ω_e can be found after expanding $\cot(kL)$ as in Eq. (26):

$$\omega_{1(2)} = \sqrt{\frac{1}{2} \left[\omega_e^2 + \omega_m^2 + g\omega_e^2 \pm \left((\omega_e + \omega_m)^2 + g\omega_e^2 \right) \left((\omega_e - \omega_m)^2 + g\omega_e^2 \right)^{1/2} \right]^{1/2}}. \quad (30)$$

When the external field H_0 is smaller than the demagnetizing field, Eq. (30) holds with $\omega_m^2 = (H_0 + (D_x - D_z)M_s)(H_0 + (D_y - D_z)M_s)$. This fact can be used to tune the FMR

frequency in order to match the elastic frequency. In this limit of strong shape anisotropy (for example a thin ferromagnetic film with $D_x \sim 4\pi$) and when $H_0 G / (M_s \beta \omega_e^2) \ll 1$, Eqs. (27,29) simplify to

$$\chi_{yy}(\omega) \approx \frac{\gamma^2 M_s^2 (D_x - D_z)}{\omega^2 - \omega_m^2 + 2i\alpha'\omega\omega_m + \omega^2 g \tan(kL)}, \quad (31)$$

$$\chi_{\varphi y}(\omega) \approx \frac{i\omega g \tan(kL)}{\omega^2 - \omega_m^2 + 2i\alpha'\omega\omega_m + \omega^2 g \tan(kL)}. \quad (32)$$

Imaginary part of $\chi_{yy}(\omega)$ corresponding to the rf absorption is plotted in Fig. 5. We observe a typical anticrossing behavior between an optically active and non-active mode, with level repulsion and transfer of oscillator strength. The intrinsic damping of the mechanical system (for MEMS Q factors can reach 10^4 , which quickly deteriorate with decreasing size, however) imposes an extra damping on the magnetization dynamics, which close to the mode crossing may dominate the intrinsic damping due to a small Gilbert constant α . In case $\beta/\omega > \alpha'$ the damping growth when we move from purely magnetic motion into purely mechanical motion along one of the lines in Fig. 4. In case $\beta/\omega < \alpha'$ the damping diminishes along such line.

The amplitude of mechanical oscillations along one of the spectrum lines in Fig. 4 is plotted in Fig. 6. The efficiency of the nanomotor is maximal at resonance.

B. Ferromagnetic cantilever

Eq. (24) describes magnetomechanical dynamics for a ferromagnetic cantilever or a dielectric cantilever covered by a ferromagnet in the whole. The LLG equation is exactly the same as in case of previous subsections apart from the fact that the torsion angle should be averaged over the cantilever. Following Eq. (24) and for frequencies close to the mechanical resonance, the coupling can be written in Fourier space as follows

$$-C\bar{\varphi} \frac{L}{2c^2} (\omega^2 + 2i\beta\omega - \omega_e^2) = \frac{V_c}{2\gamma} (-i\omega m_y - \gamma H_0 m_x) \quad (33)$$

This result is identical to the expansion in Eqs. (25,26) after substituting $V_c/2$ by V . In the expression for the coupling constant g in Eqs (27,28) we have $V/V_c = 1/2$. The coupling constant is thus increased in comparison to the case of a small magnet at the tip of the cantilever in which $V/V_c \ll 1$.

The density of a metallic single crystal cantilever (Fe) is higher $\rho \sim 8000 \text{ kg/m}^3$ and the Lamé constant $\mu \sim 100\text{GPa}^{29}$ is of the same order as for Si. Consequently, the metallic cantilever has to be smaller in order to have the same resonance frequency with the Si cantilever. Most importantly, we have to fulfill the condition $H_0 > D_z M_s$ that forces the equilibrium magnetization direction along the z -axis (alignment with the y -axis would result in zero coupling). This condition can be easily fulfilled in our geometry by not too strong magnetic fields since the largest demagnetizing factor is D_x .

It follows from Eqs. (27,28) that a ferromagnetic cantilever is more suitable for observing the magneto-mechanically coupled modes since the coupling strength is larger by the factor $V_c/2V$ compared to the system with a small magnet at the tip of the cantilever. Close to the mechanical resonance frequency both systems will behave identically.

C. Observation

The magnetovibrational coupling in our cantilever is observable by FMR and calorimetric techniques,³⁰ but the signal of nanoscale magnets is small. It might therefore be preferable to detect the resonance by the static deflection of the same cantilever due to an additional constant magnetic field \mathbf{H}_T along the x -axis, as described by Lohndorf *et al.*³¹. In our approximation the field \mathbf{H}_T creates a torque $\gamma M_y H_T \vec{x}$, whose modulation at the FMR conditions should be detectable.

Since the vibrational frequencies of state-of-the-art artificial structures are relatively low, the use of soft ferromagnets (such as permalloy), is advantageous. The magnetic mode frequencies are then determined by shape anisotropies. The FMR frequency and the mechanical resonance frequency should not differ by much more than $\Delta\omega \sim \omega\sqrt{g}$ for a pronounced effect. A Si cantilever with $a \times d \times L = (1 \times 5 \times 50) \mu\text{m}$ ($C = 10^{-13} \text{Nm}^2$) has a torsional resonance frequency of the order of $\omega_e = 10 \text{ MHz}$. Taking our ferromagnetic layer of dimensions $a_1 \times d \times \Delta L = 50\text{nm} \times 5\mu\text{m} \times 5\mu\text{m}$ (thickness, width and length), then $\omega\sqrt{g} \sim 100 \text{ KHz}$, meaning that we should tune the magnetic resonance to $\omega_e \pm 100 \text{ KHz}$ to observe the “polariton”. The necessary rf field H_x depends on the viscous dampings of mechanical and magnetization motion. At low frequencies additional sources of damping complicate measurements³² and the coherent motion of the magnetization can be hindered by domain formation. Coupling to higher resonance modes³³ or structuring of the ferromag-

net may help to carry out measurements.

An actual observation of the predicted splittings would give information about *e.g.* the magnetic moment of the film and the broadening would yield the quality factor of the elastic motion. From a technological point of view the tunable damping due to the magnetovibrational coupling might be interesting for optimizing switching speeds. A ferromagnet effectively absorbs microwaves and turns them into a precessing magnetization, which via the magnetovibrational coupling can be transformed into a coherent mechanical motion. On the other hand, the ferromagnet may interact with the mechanical motion, to cause a magnetization precession, which in turn emits polarized microwaves. The emission in the coupled regime is more energy efficient in comparison with a fixed magnetic dipole emission in the case of small Gilbert constant but relatively low mechanical quality factor. This might be interesting for *e.g.* on-chip communication applications.

In this section we have calculated the magnetic susceptibility of a system with magnetovibrational coupling by magnetocrystalline fields or via surface forces of demagnetizing currents. A condition for effective energy transfer from an external rf magnetic field into mechanical motion and *vice versa* has been established. FMR spectra are predicted to split close to the resonance, and to strongly depend on the mechanical damping. The predicted effects should be observable with existing technology, but a further reduction of system size would strongly enhance them.

IV. PROBING MAGNETIZATION DYNAMICS BY SPIN-TRANSFER TORQUES

Microwave fields are a perfect tool for probing magnetization dynamics, *e.g.* by FMR. However, with shrinking size of the magnets such methods become increasingly difficult since the power absorbed by the magnet becomes very small. In this section, we propose a method to probe the magnetization dynamics in which the role of the microwave field is taken over by spin-transfer torques. By driving an AC current through F|N|F spin valve structures with fixed and free layer magnetizations that are canted with respect to each other, we can excite the free layer motion (Fig. 7) (excitation of the magnetization motion by DC currents has already been realized³⁸). The magnetization dynamics should in turn influence the resistance of the device that can be measured. When the magnetic layer has

a mechanically active extension, as in Fig. 7, we can also detect the magneto-vibrational mode.

A. Electrical detection of FMR

We consider here F1|N|F2 multilayer structures with perpendicular magnetizations \mathbf{m}_1 and \mathbf{m}_2 assuming \mathbf{m}_2 fixed by anisotropies or exchange biasing. An AC current exerts an oscillating torque τ_1 on the magnetization \mathbf{m}_1 :³⁴

$$\frac{\tau_1}{I_0} = \frac{\hbar}{2e} \frac{1 + R_{\uparrow\downarrow}/R_1 - \beta P_1/P_2}{(1 + R_{\uparrow\downarrow}/R_1)(1 + R_{\uparrow\downarrow}/R_2) - \beta^2} \quad (34)$$

with $\beta = \cos\theta$, $4R_{1(2)} = 1/G_{1(2)\uparrow} + 1/G_{1(2)\downarrow} - 2R_{\uparrow\downarrow}$, $4R_{1(2)-} = 1/G_{1(2)\uparrow} - 1/G_{1(2)\downarrow}$, $P_{1(2)} = R_{1(2)-}/R_{1(2)}$, and $2R_{\uparrow\downarrow} = 1/G_{1\uparrow\downarrow}^r + 1/G_{2\uparrow\downarrow}^r$, where $G_{1(2)\uparrow}$ and $G_{1(2)\downarrow}$ are conductances of the left (right) ferromagnet including the left (right) normal layer, $G_{1\uparrow\downarrow}^r$ and $G_{2\uparrow\downarrow}^r$ are mixing conductances of the middle normal metal with adjacent ferromagnet interfaces. The resulting magnetization dynamics causes oscillations of the resistance of the multilayer structure according to³⁴

$$\Re(\theta) = R + R_1 + R_2 - \frac{R_{\uparrow\downarrow}(R_{1-} + \beta R_{2-})^2 + (1 - \beta^2)(R_{1-}^2 R_2 + R_{2-}^2 (R_1 + R_{\uparrow\downarrow}))}{(R_{\uparrow\downarrow} + R_1)(R_{\uparrow\downarrow} + R_2) - \beta^2 R_1 R_2}. \quad (35)$$

In the following, we consider only small deviations of \mathbf{m}_1 from the perpendicular to \mathbf{m}_2 direction. All the equations can then be rewritten keeping only the leading terms with respect to small β . The torque τ_1 is proportional to the current I_0 in this approximation:

$$\tau_1 = I_0 \frac{\hbar}{2e} \frac{1 + R_{\uparrow\downarrow}/R_1}{(1 + R_{\uparrow\downarrow}/R_1)(1 + R_{\uparrow\downarrow}/R_2)} = V |\mathbf{M} \times \mathbf{H}_x| \quad (36)$$

where we defined an effective rf field \mathbf{H}_x along the axis x that creates the same torque as the oscillating AC current. Thus the response function $(m_y/I_0)_\omega = K\chi_{yx}(\omega)$ with

$$KM_s V = \frac{\hbar}{2e} \frac{1 + R_{\uparrow\downarrow}/R_1}{(1 + R_{\uparrow\downarrow}/R_1)(1 + R_{\uparrow\downarrow}/R_2)}, \quad (37)$$

and the susceptibility can be found from Eq. (4). To the first order in the mechanical damping constant β we can write the dynamical impedance as:

$$Z(\omega) = R + R_1 + R_2 - \frac{R_{\uparrow\downarrow}(R_{1-}^2 + 2I_0 K \chi_{yx}(\omega) R_{2-} R_{1-}) + (R_{1-}^2 R_2 + R_{2-}^2 (R_1 + R_{\uparrow\downarrow}))}{(R_{\uparrow\downarrow} + R_1)(R_{\uparrow\downarrow} + R_2)}. \quad (38)$$

$|Z(\omega)|$ normalized by the resistance of the locked perpendicular magnetizations is plotted in Fig. 8. The parameters of the spin valve are the same with the symmetric setup of ref.³⁴ The

current amplitude I_0 is chosen to correspond to magnetization oscillations of 15 degrees which appears to be readily experimentally accessible. In Fig. 8 the FMR resonance corresponds to the dip in the absolute value of the impedance that should be easily detectable.

B. Electrical detection of magnetovibrational mode

The method described in the previous chapter can also be used for detecting the magnetovibrational modes. The ferromagnet F1 is extended forming a ferromagnetic cantilever (Fig. 7). The magnetization \mathbf{m}_2 can have two directions (bold and dashed lines in Fig. 7) that are equally suitable for this purpose. In principle, the direction plotted by dashed line can cause a constant torsion of the cantilever when a constant current is sent through the spin valve since in this case the spin-transfer torque is transferred to the mechanical torque via the shape anisotropy. We concentrate here on the direction of \mathbf{m}_2 indicated by the bold arrow which can be easier realized in experiment. When an AC current is sent through the system the oscillating torque causes oscillations of the magnetization \mathbf{m}_1 as explained in the previous section. At resonance, we can observe the magnetovibrational mode as a splitting of the dip in the absolute value of the impedance plotted in Fig. 9. The width of the dips is a measure of the damping that is approximately half of the width in Fig. 8 for chosen parameters, which is consistent with the results of Sec 3.1 .

In a long cantilever with a finite exchange stiffness, the macrospin magnetization motion can be complicated by spin waves. The effective field for the LLG Eq. (1) in the presence of nonuniform magnetization reads

$$\mathbf{H}_{\text{eff}} = -D_x M_x \mathbf{x} - D_y M_y \mathbf{y} - D_z M_z \mathbf{z} + \frac{2A}{M_s^2} \nabla^2 \mathbf{M} + \mathbf{H}_0 \quad (39)$$

where A is the exchange stiffness. The lowest-energy bulk spin wave mode is along the cantilever with the frequency that can be found from the LLG equation written in Fourier space:

$$\begin{bmatrix} -i\omega & \gamma(\frac{2A}{M_s}k^2 + (D_y - D_z)M_s + H_0) \\ -\gamma(\frac{2A}{M_s}k^2 + (D_x - D_z)M_s + H_0) & -i\omega \end{bmatrix} \begin{bmatrix} m_x/M_s \\ m_y/M_s \end{bmatrix} = 0 \quad (40)$$

where $\mathbf{M} = (m_x \mathbf{x} + m_y \mathbf{y})e^{i(\omega t + \mathbf{k} \cdot \mathbf{r})} + M_s \mathbf{z}$. The resonance frequency is $\omega_{sw} = \gamma \sqrt{(\frac{2A}{M_s}k^2 + (D_x - D_z)M_s + H_0)(\frac{2A}{M_s}k^2 + (D_y - D_z)M_s + H_0)}$. We estimate the difference

between frequencies of the macrospin mode with $k = 0$ and the longest wavelength mode with $k = \pi/L$. For a thin film $\gamma\sqrt{4\pi M_s \frac{2A}{M_s} (\pi/L)^2} \approx 0.2$ GHz, where we adopted $A = 2 \times 10^{-11}$ J/m, $M_s = 1.4 \times 10^6$ A/m and $L = 1$ μ m. Since we excite the mechanical motion monochromatically by the AC currents, it is sufficient then to have the mode splitting larger than the broadening. This shows that in principle we can design the magnetic and mechanical subsystems to avoid bulk spin wave generation provided the mechanical damping as well as the Gilbert damping are relatively small. Note that by applying an antiferromagnetic layer on top of the cantilever we can strengthen exchange stiffness thus diminishing the possibility of spin waves even further.

It is also possible to include coupling of the mechanical motion to spin waves but this regime will not be considered here.

V. LARGE MAGNETIZATION CONES AND MAGNETIZATION REVERSAL IN THE PRESENCE OF COUPLING

In this section, we extend the linearized magnetization motion to large angles relevant *e.g.* for the magnetization reversal.

A. Resonant magnetization oscillations and reversal

We consider resonant oscillations of the mechanical and magnetic degrees of freedom. We restrict ourself here to the case when only one anisotropy direction is present (*e.g.* $D_y = D_z = 0$) which is relevant for very thin ferromagnetic films with an easy plane anisotropy when $D_x \sim 4\pi$.

The coupling of Eqs. (1) and (17) is

$$\begin{aligned} \frac{\partial \varphi}{\partial y} \Big|_{y=L} &= \frac{1}{C\gamma} \left(\frac{dM_y}{dt} + \gamma \mathbf{M} \times \mathbf{H}_0 \Big|_y \right), \\ \mathbf{H}_{\text{eff}} &= (D_x M_z \varphi - D_x M_x) \mathbf{x} + D_x M_x \varphi \mathbf{z} + \mathbf{H}_0, \end{aligned} \quad (41)$$

We first address the maximal possible coupling strength of a system described by Eq. (41). Consider the two subsystems oscillating at a common frequency ω . The total mechanical energy is then $E_{me} = \rho I L \omega^2 \varphi_0^2$, where φ_0 is the maximal angle of the torsional motion. By equipartition this energy should be of the order of the magnetic energy $E_{mg} = M_s V H_0$. The maximal angle would correspond to the mechanical motion induced by full transfer

of the magnetic energy to the lattice. By equalizing those energies, we find an estimate for the maximal angle of torsion $\varphi_0 = \sqrt{M_s V H_0 / (\rho I L \omega^2)}$. The coupling between the subsystems can be measured by the distribution of an applied external torque (*e.g.* applied by a magnetic field) over the two subsystems. The total angular momentum flow into the magnetic subsystem by the effective magnetic field is $(M_s V / \gamma) \omega$, whereas that corresponding to the mechanical subsystem at the same frequency is $(\rho I L \omega \varphi_0) \omega$. Their ratio is $\varphi_0 \omega / (\gamma H_0)$. The maximum angle φ_0 derived above is therefore also a measure of the coupling between the magnetic and mechanical subsystems. This estimate is consistent with the coupling strength of polariton modes at resonance of $g = \varphi_0^2 \omega^2 / (\gamma H_0)^2 \approx \varphi_0^2 D_x M_s / H_0$ in Eqs. (27,28) (in this estimate we consider the case of not too strong external fields when $\omega \approx \gamma \sqrt{H_0 D_x M_s}$). An estimate for a cantilever with $\rho = 2330 \text{ kg/m}^3$ (Si) and $d = 100 \text{ nm}$ ($\omega \sim 1 \text{ GHz}$) leads to $g = \varphi_0^2 D_x M_s / H_0 \sim (L/a)^2 (M_s^2 / \mu) \sim 10^{-3}$. Increasing (L/a) and M_s or decreasing Lamé constant μ is beneficial for the coupling.

Magnetization reversal by a magnetic field in the coupling regime can be realized even without any damping by transferring magnetic energy into the mechanical system. Since we find that $\varphi_0 \ll 1$ for realistic parameters, the subsystems undergo many precessions/oscillations before the switching is completed. The switching is then associated with a slow time scale corresponding to the global motion governed by the coupling or a weak damping relative to a fast time scale characterized by the Larmor frequency. The equation of motion for the slow dynamics (the envelope functions) can be derived by averaging over the rapid oscillations. To this end, we substitute LLG Eq. (19) and first of Eqs. (41), linearized in the small parameters α , β and φ_0 , into the equations for the mechanical and the magnetic energies:

$$\begin{aligned} \frac{d}{dt} E_{me} &= -2\beta E_{me} + C\tau|_{x=L} \frac{d\varphi}{dt}|_{x=L}, \\ \frac{d}{dt} E_{mg} &= -H_0 \dot{M}_z + D_x M_x \dot{M}_x. \end{aligned} \quad (42)$$

We focus in the following on the regime $H_0 \ll D_x M_s$, which usually holds for thin films and not too strong fields, in which the magnetization motion is elliptical with long axis in the plane and small M_x even for larger precession cones. Disregarding terms containing higher powers of M_x and averaging over one period as indicated by $\langle \dots \rangle$

$$\begin{aligned} \left\langle \frac{dE_{me}}{dt} \right\rangle + \langle 2\beta E_{me} \rangle &= -V D_x \langle M_z M_x \dot{\varphi} \rangle, \\ \left\langle \frac{dE_{mg}}{dt} \right\rangle + \langle \alpha D_x^2 M_s M_x^2 \rangle &= D_x \langle M_z \dot{M}_x \varphi \rangle. \end{aligned} \quad (43)$$

By adiabatic shaping of time-dependent magnetic fields $H_0(t)$ we can keep the two subsystems at resonance at all times ($H_0(t)$ does not change much since we do not consider large angle cones that are very close to the antiparallel configuration). The slow dynamics $\varphi(L, t) \sim A(t)e^{i(\omega+\pi/2)t}$ and $M_x \sim W(t)e^{i\omega t}$ in time domain is then governed by the equation:

$$\begin{aligned}\dot{A} + \beta A &= -g\omega_m/M_s(-1 + \frac{D_x W^2}{4M_s H_0})W, \\ \dot{W} + \alpha'\omega W &= \omega M_s(-1 + \frac{D_x W^2}{4M_s H_0})A,\end{aligned}\tag{44}$$

we introduced a frequency $\omega_m = \gamma\sqrt{D_x M_s H_0(t)}$ that at $t = 0$ coincides with the frequency of fast oscillations ω . Substitutions $\varphi(L, t) \sim \tilde{A}(t)e^{i\omega t}$ and $M_x \sim \tilde{W}(t)e^{i(\omega-\pi/2)t}$ corresponding to $\pi/2$ -shifted harmonics are also solutions, and the initial conditions determine the linear combination of two envelope functions, *i.e.* the beating pattern of two hybridized polariton modes⁹. When initially all energy is stored in one degree of freedom, M_x is $\pi/2$ shifted from $\varphi(L, t)$ and $A_2(t) = 0$. Eqs. (44) describe a (damped) harmonic oscillator with frequency $\sqrt{g\bar{\omega}_m\omega} \ll \omega$ when $D_x W/4 \ll MH_0$ (since ω_m does not change much we replaced it by averaged $\bar{\omega}_m$). Such oscillatory behavior persists for general angles (except for motion with very large angle cones close to the antiparallel configuration). This is illustrated by Fig. 10 which shows a numerical simulation of Eq. (22) for an undamped system excited at $t = 0$ by a magnetic field \mathbf{H}_0 at an angle $2\pi/3$ with the initial magnetization. The number of periods necessary to transfer all energy from one subsystem to the other is therefore given by $\sim 1/(4\sqrt{g})$. Eq. (44) also shows that for damping constants $\alpha > \varphi_0/\pi$ or $\beta/\omega > \sqrt{g}/\pi$ the beating is suppressed.

Fig. 10 illustrates that the mechanical system absorbs energy from the magnetic subsystem and gives it back repeatedly in terms of violent oscillations that are modulated by an envelope function on the time scale derived above in Eq. (44) as plotted by dotted line. When the envelope function vanishes the magnetization is reversed and the systems seems to be at rest. However, since the energy is not dissipated, the momentarily silence is deceptive, and the beating pattern repeats. An efficient coupling requires that the frequencies of the subsystems are close to each other at each configuration, which was achieved in the simulation by the adiabatic modulation of the magnetic field H_0 according to Fig. 2. However, the reversal process is robust; an estimate from Eqs. (43) for the necessary proximity of the resonant frequencies of the mechanical and the magnetic subsystems is $\Delta\omega \sim \sqrt{g}\omega$. In that case, the above estimates still hold.

Let us now consider the magnetization reversal by an antiparallel magnetic field $H_0(t)$ that undergo slow change of amplitude to keep the subsystems at resonance. This method of magnetization reversal by oscillating demagnetizing field due to mechanical oscillations is strongly analogous to the reversal by time-dependent magnetic fields.²⁵ However, in contrast to the time-dependent field reversal, we vary the field $H_0(t)$ but not the rf fields so avoiding complicated time dependence of rf fields.²⁵ We can calculate the dependence $H_0(t)$ in advance for a specific sample, or we can create feedback circuit by connecting metallic contacts to the magnetic film, thus monitoring the dynamics. Since we assume zero temperature, the dynamics in Fig. 11 is initiated by assuming a tiny angle of magnetization at $t = 0$. We wish to illustrate here that making use of the magnetoelastic coupling can accelerate the reversal importantly. We can suppress the backflow of mechanical energy for example by a sufficiently damped mechanical subsystem, as evident in Fig. 6 by comparing the two curves for $\beta \sim 0$ and $\beta \sim 0.02$ with vanishing Gilbert damping, $\alpha = 0$. Alternatively, we may detune the external magnetic field out of the resonance precisely after the first reversal, effectively rectifying the energy flow from the magnetic into the mechanical subsystem. We observe that even without any intrinsic damping ($\alpha = \beta = 0$) the unwanted “ringing” can be strongly suppressed (dashed line in Fig. 6).

The experimental realization of such magnetization reversal will be a challenge since the cantilever has to preferably work at high frequencies ~ 1 GHz. In the resonant reversal, a significant coupling strength of $g \sim 10^{-3}$ requires that one tenths of the cantilever volume is a ferromagnet. We investigated here the non-linear dynamics of coupled magnetic and mechanical fields for a cantilever with a ferromagnetic tip. Employing the new dissipation channels, we propose new strategies for fast magnetization reversal and suppressed “ringing”. We can make use of the additional mechanical damping or shape the external magnetic field pulses, thus quickly channeling-off magnetic energy when damping is weak.

B. Non-resonant magnetization oscillations and reversal

We propose a non-resonant mechanical reversal scheme analogous to “precessional” switching¹³. The effective field \mathbf{H}_{eff} (see Eq. (22)) has a component perpendicular to the plane of the film $H_x \sim M\varphi$. Under a sudden mechanical twist this component acts like a transverse magnetic pulse about which the precessing develops. Alternatively, we can

suddenly release a twist preinstalled on the cantilever. This could be achieved by an STM tip bonded to an edge of the cantilever at (L, d) and pulling it up slowly to the breaking point. The mechanical response should be fast, *i.e.* react on a time scale $(\gamma\varphi\nu M)^{-1}$, but there are no resonance restrictions now. We integrate the equation of motion numerically for a strongly damped cantilever $\beta/\omega \sim 0.15$ initially twisted by $\varphi = 0.2$ and suddenly released at $t = 0$. We reintroduce an easy axis anisotropy described by $DM_z\mathbf{z}$. Adopt $D = 0.05$, $\alpha = 0.01$ and no external fields. Fig. 12 displays the desired reversal. The rather severe overshoot, as in the case of the precessional switching technique, can be minimized by carefully engineering the mechanical actuation to be closer to the optimum “ballistic“ path between $M_z = \pm 1$.

Summarizing, we demonstrate here a precessional reversal scheme based on the mechanically generated out-of-plane demagnetizing field without applied magnetic fields. In this reversal scheme, the sharp control of the resonance condition is not required, however, the cantilever has to be fast determining the reversal time.

VI. CONCLUSION

This paper reports a detailed study of magnetomechanical effects in small magnetic cantilevers, summarizing some old results^{9,10} and making several generalizations. We proved that for small magnetization oscillations close to the mechanical resonance frequency, a ferromagnetic cantilever behaves like the dielectric cantilever with a small magnet at the tip analyzed before. Such a ferromagnetic cantilever has an enhanced coupling of mechanical and magnetic degrees of freedom and thus is more suitable for observation of magnetomechanical effects. A metallic ferromagnetic cantilever can be integrated into magnetoelectronic circuits as shown in Sec. IV. Such an integrated device has the potential as a fast transducer of mechanical motion as an alternative to previous designs that take advantage of magnetomotive forces. In our case, the magnetomotive forces are supplanted by spin-transfer torques. Our strategy; that is to say to avoid magnetic fields, is similar to what happens in the field of random access memories in which there is a considerable effort to replace magnetic fields by employing spin-transfer torques. The technique presented in this paper strongly relies on resonant magnetovibrational coupling in which the magnetic torques can be effectively transformed into mechanical torques and *vice versa*. In order to see magnetomechanical torques

in experiment, one needs to be able to handle small structures on micro and nano scale, the magnets have to be small enough to form a single domain. We believe that the integration of magnetoelectronics and magnetomechanics is possible and should lead to devices with new functionalities.

Acknowledgment

We thank Yaroslav Tserkovnyak for helpful discussions. This work has been supported by the Dutch FOM Foundation and the Research Council of Norway.

Figure 1: A magnetomechanical cantilever supporting magneto-vibrational modes. On a dielectric substrate (such as Si) a single-domain ferromagnetic film is deposited at the free end.

Figure 2: Dependence of FMR broadening on aspect ratio $m = a/c$ for ellipsoid with the semi-axes a and $b = c$ ($H_0 = M_s$).

-
- ¹ M. L. Roukes, Phys. World **14** (2), 25 (2001).
- ² K. C. Schwab and M. L. Roukes, Phys. Today, July 2005.
- ³ J. A. Sidles, J. L. Garbini, K. J. Bruland, D. Rugar, O. Zuger, S. Hoen and C.S. Yannoni, Rev. Mod. Phys. **67**, 249 (1995).
- ⁴ X. M. H. Huang, C. A. Zorman, M. Mehregany, and M. Roukes, Nature (London) **421**, 496 (2003).
- ⁵ C. Friedsam, A. K. Wehle, F. Kühner and H. E. Gaub, J. Phys. Condens. Matter **15**, S1709 (2003).
- ⁶ K. L. Ekinci, Y. T. Yang, M. L. Roukes, J. Appl. Phys. **95**, 2682 (2004).
- ⁷ D. Rugar, R. Budakian, H. J. Mamin and B. W. Chui, Nature **430**, 329 (2004).
- ⁸ I. Bargatin and M.L. Roukes, Phys. Rev. Lett. **91**, 138302 (2003).
- ⁹ A.A. Kovalev, G.E.W. Bauer and A. Brataas, Appl. Phys. Lett. **83**, 1584 (2003).
- ¹⁰ A. A. Kovalev, G.E.W. Bauer and A. Brataas, Phys. Rev. Lett. **94**, 167201 (2005).
- ¹¹ B. Hillebrands and K. Ounadjela (Eds.), *Spin Dynamics in Confined Magnetic Structures*, (Springer, Berlin, 2003); S. Maekawa and T. Shinjo (Eds.), *Applications of Magnetic Nanostructures*, (Taylor and Francis, New York, 2002).
- ¹² M. Jamet, W. Wernsdorfer, C. Thirion, V. Dupuis, P. Mélinon, A. Pérez and D. Mailly, Phys. Rev. B **69** (2), 024401 (2004).

Figure 3: The period T_1 ($E_{mg} < 1$) and T_2 ($E_{mg} > 1$) of the magnetization dynamics in Eqs. (15) in units $2\pi / (\gamma\sqrt{(H_0 + D_x M)H_0})$ as a function of energy in units $H_0 M$. The inset shows a plot of typical trajectories at different energies on the unit sphere ($D_x M = 10H_0$).

Figure 4: Dependence of the resonance frequency of the coupled motion on the FMR frequency ω_m of the uncoupled magnetization ($g \sim 0.001$).

Figure 5: The oscillator strength corresponding to each resonance in Fig. 4 in arbitrary units plotted by full lines and their widths plotted by dashed lines ($g \sim 0.001$, $\beta/\omega > \alpha'$).

- ¹³ Th. Gerrits, H.A.M. van den Berg, J. Hohlfeld, L. Bär, and Th. Rasing, *Nature* **418**, 509 (2002).
- ¹⁴ C. H. Back, D. Weller, J. Heidmann, D. Mauri, D. Guarisco, E. L. Garwin and H. C. Siegmann, *Phys. Rev. Lett.* **81**, 3251 (1998).
- ¹⁵ H. W. Schumacher, C. Chappert, P. Crozat, R. C. Sousa, P. P. Freitas, J. Miltat, J. Fassbender and B. Hillebrands, *Phys. Rev. Lett.* **90**, 0117201 (2003).
- ¹⁶ J.C. Slonczewski, *J. Magn. Magn. Mater.* **159**, L1 (1996); L. Berger, *Phys. Rev. B* **54**, 9353 (1996).
- ¹⁷ M. Tsoi, A. G. M. Jansen, J. Bass, W.-C. Chiang, M. Seck, V. Tsoi and P. Wyder, *Phys. Rev. Lett.* **80**, 4281 (1998).
- ¹⁸ T. Valet, unpublished.
- ¹⁹ A. Yamaguchi, T. Ono, S. Nasu, K. Miyake, K. Mibu and T. Shinjo, *Phys. Rev. Lett.* **92**, 077205 (2004); G. Tatara and H. Kohno *Phys. Rev. Lett.* **92**, 086601 (2004); S.E. Barnes and S. Maekawa, *cond-mat/0311039*.
- ²⁰ J-E Wegrowe, D. Kelly, Y. Jaccard, Ph. Guittienne, J-Ph Ansermet, *Europhys. Lett.* **45**, 626 (1999).
- ²¹ J.Z. Sun, *J. Magn. Magn. Mater.* **202**, 157 (1999).
- ²² E. B. Myers, D. C. Ralph, J. A. Katine, R. N. Louie, R. A. Buhrman, *Science* **285**, 867(1999).
- ²³ S. I. Kiselev, J. C. Sankey, I. N. Krivorotov, N. C. Emley, R. J. Schoelkopf, R. A. Buhrman and D. C. Ralph, *Nature* **425** (6956), 380 (2003).
- ²⁴ A. V. Kimel, A. Kirilyuk, A. Tsvetkov, R. V. Pisarev and Th. Rasing, *Nature* **429**, 850 (2004).
- ²⁵ Z. Z. Sun and X. R. Wang, preprint (2005).
- ²⁶ T.L. Gilbert, *Phys. Rev.* **100**, 1243 (1955); *IEEE Trans. Magn.* **40**, 3443 (2004).

Figure 6: Amplitude of mechanical oscillations along one of the resonances in Fig. 4. The maximal efficiency of the "nanomotor" occurs when both subsystems are at resonance.

Figure 7: Electro-magneto-mechanical device.

Figure 8: Dependence of the normalized impedance on the AC current frequency ($\alpha' = 0.02$).

- ²⁷ C. Serpico, I.D. Mayergoyz and G. Bertotti, *J. Appl. Phys.* **93**, 6909 (2003).
- ²⁸ L.D. Landau and E.M. Lifshitz, *Theory of Elasticity*, 2nd ed. (Pergamon, Oxford, 1959).
- ²⁹ M. G. Simmons and H. Wang, Single crystal elastic constants and calculated aggregate properties, MIT Press, 1975. J. D. Bass, Elasticity of Minerals, Glasses, and Melts, pp.45-63, in *Mineral Physics and crystallography: a handbook of physical constants*, edited by T. J. Ahrens, AGU, Washington, DC., 1995.
- ³⁰ J. Moreland, M. Lohndorf, P. Kabos, and R. D. McMichael, *Rev. Sci. Instrum.* **71**, 3099 (2000).
- ³¹ M. Lohndorf, J. Moreland, and P. Kabos, *Appl. Phys. Lett.* **76**, 1176 (2000).
- ³² G. F. Cochran, R. W. Qiao, and B. Heinrich, *Phys. Rev. B* **39**, 4399 (1989).
- ³³ U. Rabe, K. Janser, and W. Arnold, *Rev. Sci. Instrum.* **67**, 3281 (1996).
- ³⁴ A. A. Kovalev, A. Brataas, and G. E. W. Bauer, *Phys. Rev. B* **66**, 224424 (2002).
- ³⁵ T. Ono, H. Miyajima, K. Shigeto, K. Mibu, N. Hosoi, T. Shinjo, *Science* **284** (5413), 468 (1999).
- ³⁶ M. Tsoi, R.E. Fontana, S.S.P. Parkin, *Appl. Phys. Lett.* **83**, 2617 (2003).
- ³⁷ D. Atkinson, D. A. Allwood, G. Xiong, M. D. Cooke, C. C. Faulkner and R. P. Cowburn, *Nature Materials* **2**, 85 (2003).
- ³⁸ I. N. Krivorotov, N. C. Emley, J. C. Sankey, S. I. Kiselev, D. C. Ralph, and R. A. Buhrman, *Science* **307**, 228 (2005).
- ³⁹ A.N. Cleland, *Foundations of Nanomechanics* (Springer-Verlag, 2002).
- ⁴⁰ P.B. Visscher and X. Feng, *Phys. Rev. B* **65**, 104412 (2002).
- ⁴¹ S. Wolf, D. D. Awschalom, R. Buhrman, J. Daughton, S. von Molnar, M. Roukes, A. Chtchelkanova, and D. Treger, *Science* **294**, 1488 (2001).
- ⁴² S. S. P. Parkin, *Applications of Magnetic Nanostructures* (Taylor and Francis, New York, 2002), p. 237.

Figure 9: Dependence of the normalized impedance on the AC current frequency ($\omega_m = \omega_e$, $\alpha' = 0.02$, $\beta/\omega = 0.002$).

Figure 10: Time-dependent response of the magnetomechanical system to an external magnetic field switched on at $t = 0$ at an angle $2\pi/3$ with the initial magnetization, in the absence of dissipation. Plotted are the $\varphi(L)$ and z -components of the magnetization ($D_x M = 10H_0$).

Figure 11: Time-dependent response of the magnetomechanical system to an external magnetic field switched on at $t = 0$ ($D_x M = 10H_0$, $\alpha = 0$). The importance of mechanical damping can be seen by comparing the dotted line ($\beta = 0$) with the full line ($\beta = 0.02$). The dashed line illustrates the dynamics when the subsystems brought out of resonance by reducing the external magnetic field to half of its initial value at $t = 6.5$ ($\beta = 0$).

⁴³ A. Jander, J. Moreland, and P. Kabos, Appl. Phys. Lett. **78**, 2348 (2001).

⁴⁴ O. Benda, IEEE Trans. Mag. **5**, 921 (1969).

Figure 12: Magnetization switching without external field by an initially twisted cantilever that is released at $t = 0$. The inset shows the corresponding magnetization trajectory on the unit sphere.

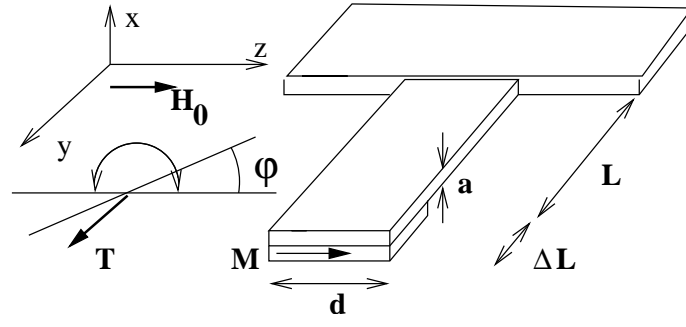


Fig. 1

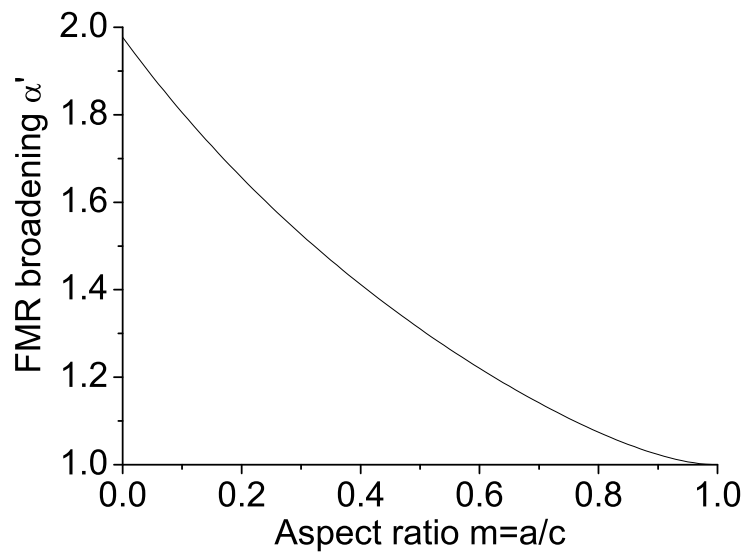


Fig. 2

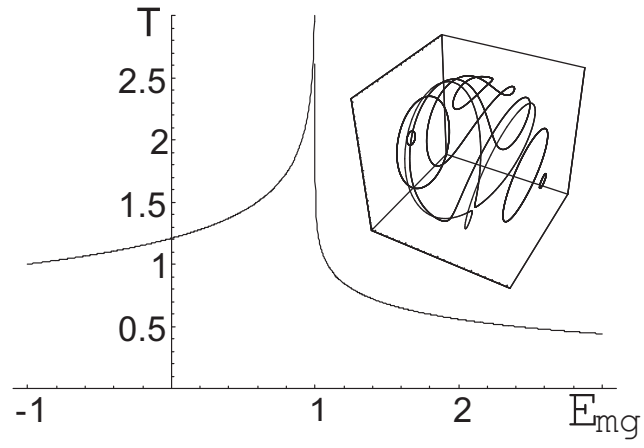


Fig. 3

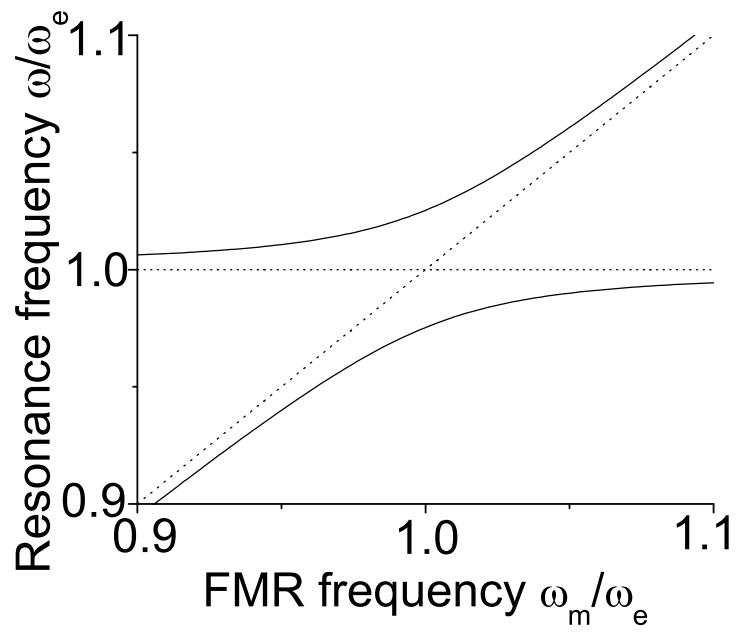


Fig. 4

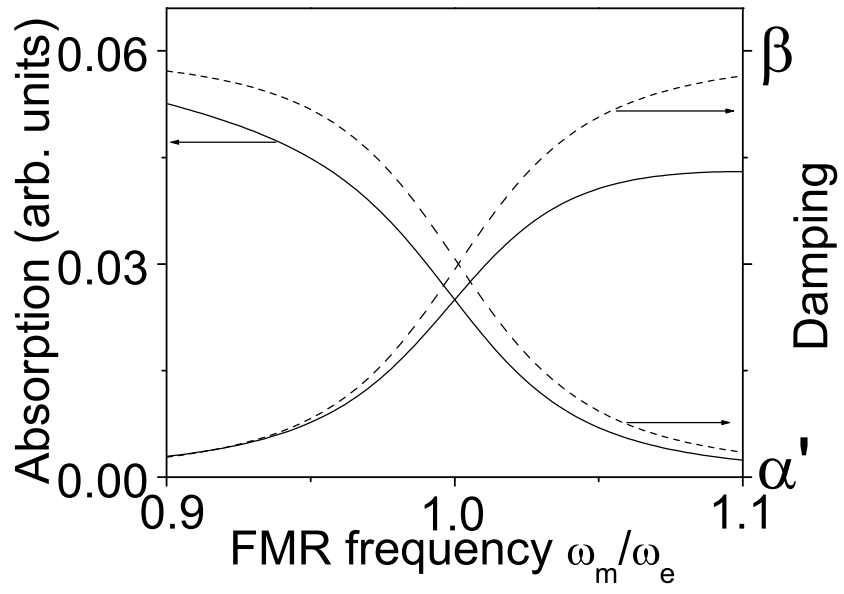


Fig. 5

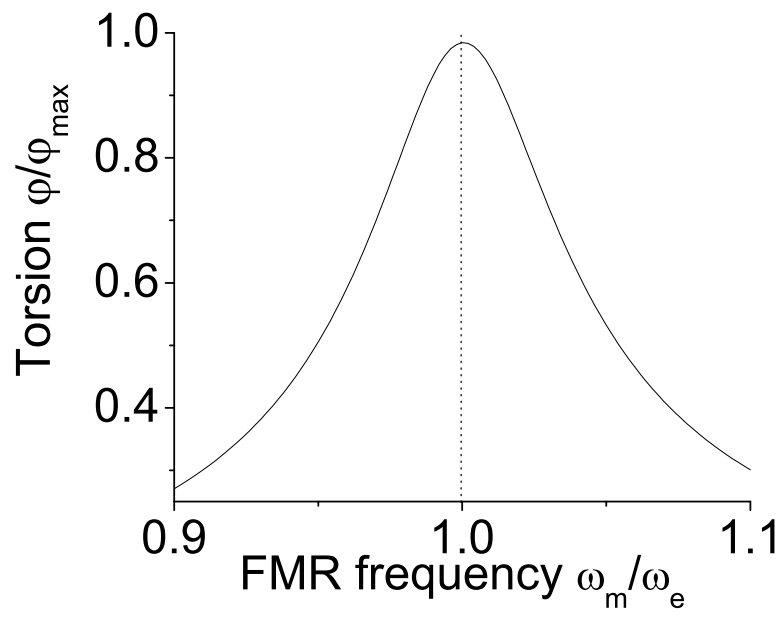


Fig. 6

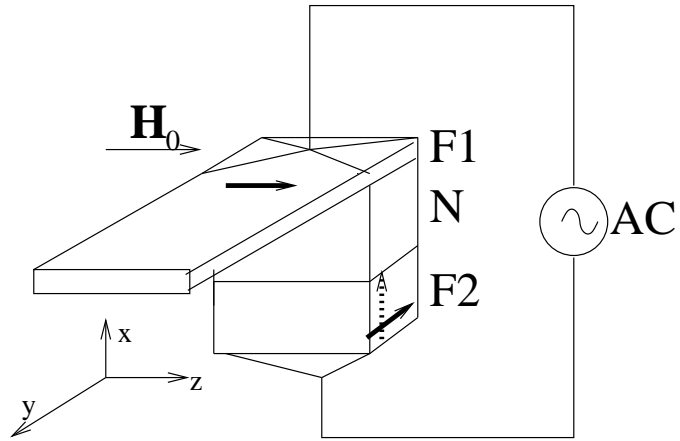


Fig. 7

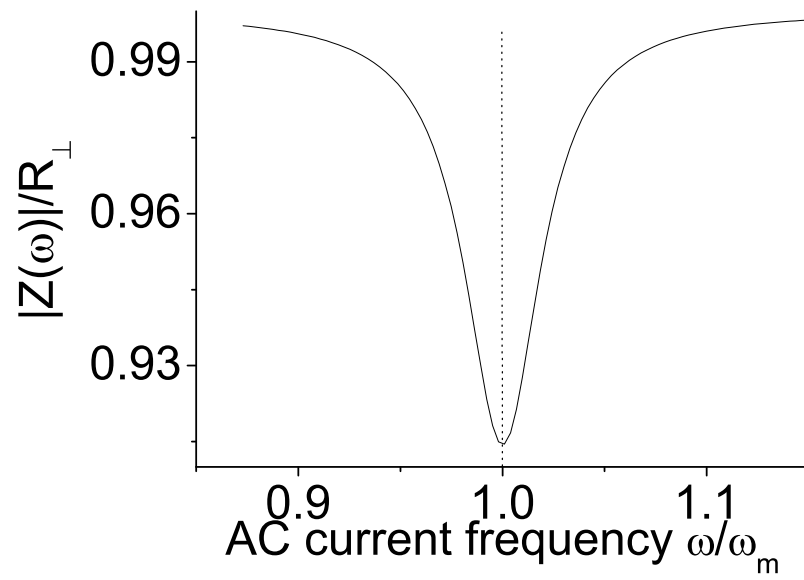


Fig. 8

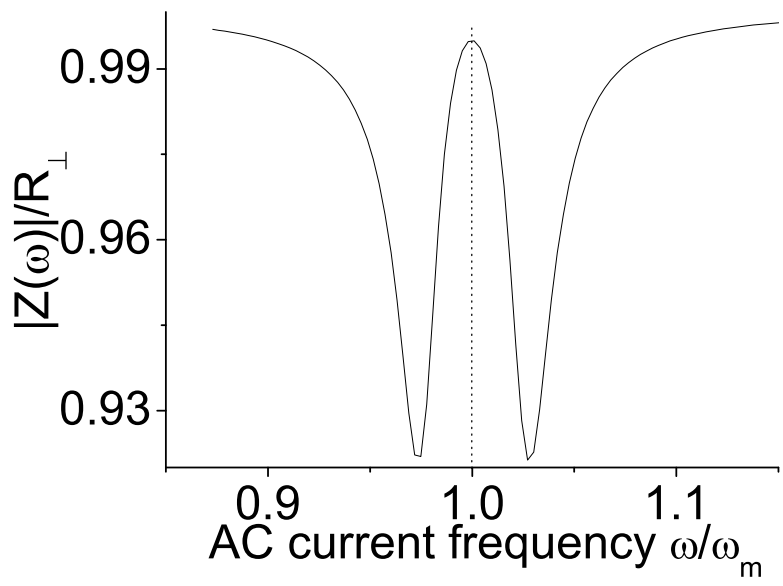


Fig. 9

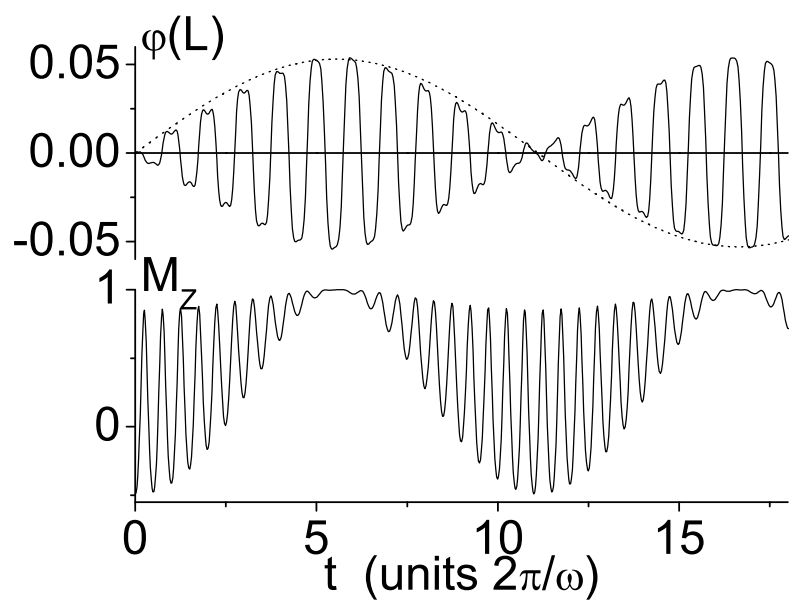


Fig. 10

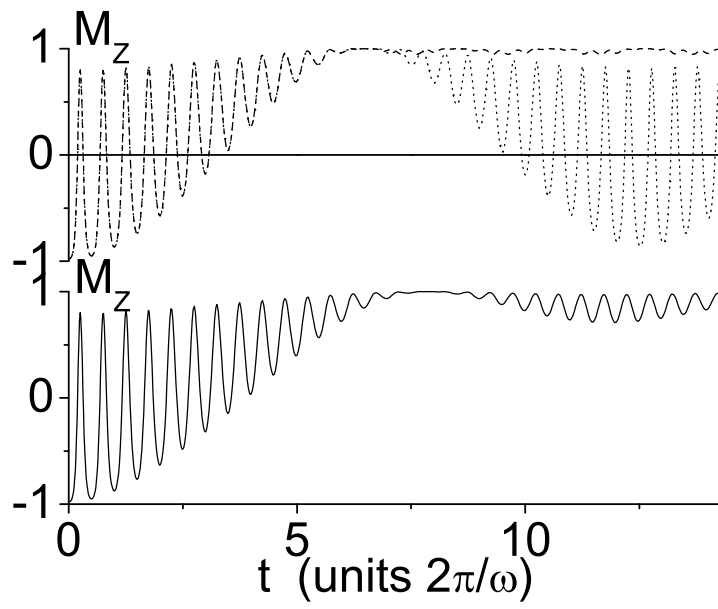


Fig. 11

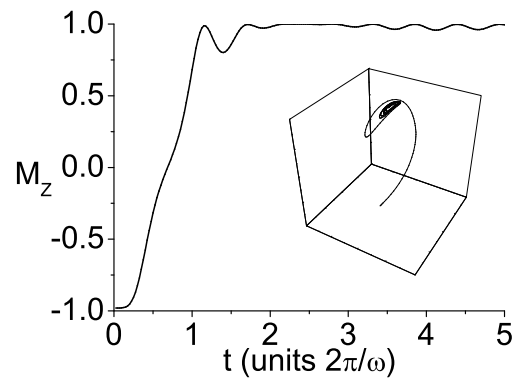


Fig. 12